Efficient Stabilized Two-Qubit Gates on a Trapped-Ion Quantum Computer

Reinhold Blümel,[1,2] Nikodem Grzesiak,[2] Nhung H. Nguyen,[3] Alaina M. Green,[3] Ming Li,[2] Andrii Maksymov,[2] Norbert M. Linke,[3] and Yunseong Nam[2,3]

[1]*Wesleyan University, Middletown, Connecticut 06459, USA*
[2]*IonQ, College Park, Maryland 20740, USA*
[3]*Joint Quantum Institute, University of Maryland, College Park, Maryland 20742, USA*

(Received 22 January 2021; accepted 4 May 2021; published 4 June 2021)

In order to scale up quantum processors and achieve a quantum advantage, it is crucial to economize on the power requirement of two-qubit gates, make them robust to drift in experimental parameters, and shorten the gate times. Applicable to all quantum computer architectures whose two-qubit gates rely on phase-space closure, we present here a new gate-optimizing principle according to which negligible amounts of gate fidelity are traded for substantial savings in power, which, in turn, can be traded for substantial increases in gate speed and/or qubit connectivity. As a concrete example, we illustrate the method by constructing optimal pulses for entangling gates on a pair of ions within a trapped-ion chain, one of the leading quantum computing architectures. Our method is direct, noniterative, and linear, and, in some parameter regimes, constructs gate-steering pulses requiring up to an order of magnitude less power than the standard method. Additionally, our method provides increased robustness to mode drift. We verify the new trade-off principle experimentally on our trapped-ion quantum computer.

DOI: 10.1103/PhysRevLett.126.220503

Introduction.—For the growing number of programmable quantum computers available today [1–10], computational instructions for quantum applications are typically compiled into single- and two-qubit quantum gates [11–13]. In all current quantum-computer architectures, two-qubit gates are about 1 to 2 orders of magnitude more costly to implement than single qubit gates in terms of the required power, fidelity, and gate speed [14,15]. Therefore, improving two-qubit gate performance is critical to the utility and scalability of quantum computers. While it is too early to predict which qubit realization technology will ultimately be used to construct the most powerful quantum supercomputers, a large portion of today's most advanced quantum computers [1–10] is realized either with superconducting or trapped-ion qubits. In the realm of trapped-ion qubits, both quantum charge coupled device technology (QCCD) [4] and trapped ion-string technology [4–8,16] have successfully been realized. We focus in this Letter on ion-string technology as a test bed for our methods, although the methods are generally applicable to QCCD technology as well. Within the framework of ion-string technology, the best two-qubit gates are mediated by the harmonic motion through spin-dependent forces [17–22]. For laser-based gates in multi-ion chains, a range of pulse-shaping protocols has been devised to decouple the multiple motional modes from the qubit degrees of freedom, such as amplitude modulation [7,23–26], phase modulation [27–29], frequency modulation [30], or combinations thereof [31,32]. These pulses can also create additional resilience to mode drift [31,32] and gate-timing errors [32], enable fast gate action [33], or allow for simultaneous [34,35] or multiqubit [36] gates.

In Ref. [31], based on the Mølmer-Sørensen protocol [18–20], we presented a constructive method for calculating power-optimal pulse shapes with perfect fidelity. In practice, however, we expect a quantum gate to be imperfect due to limitations independent of the pulse shape, such as intensity fluctuations due to beam-power or beam-steering noise, motional-mode heating, motional dephasing, laser dephasing, off-resonant photon scattering, qubit dephasing or depolarization, and others. Therefore, we need not require mathematical exactness in constructing the pulse shape, but rather ensure that the error incurred by the imperfect pulse shape is much smaller than the other error mechanisms limiting the fidelity. Based on this strategy we present here a pulse-shaping technique that includes a systematic method of trading negligible amounts of fidelity for power savings of up to an order of magnitude under realistic operating conditions on our trapped-ion quantum computer. Alternatively, by trading power savings for gate speed, we are able to speed up two-qubit gates for a given power budget. We confirm this new trade-off principle experimentally on our trapped-ion quantum computer. This method also constructs gates that are naturally robust to mode-frequency drifts. We emphasize that our methods are generally applicable to all gate schemes that rely on phase-space closure and work for all gate types, such as XX [5,7,31] and ZZ [37,38] gates.

Protocol.—Implementation of the trade-off strategy is based on a provably power-optimal pulse-shaping method

for laser-based radial-mode gates [31]. Using simultaneous amplitude and frequency modulation, including stabilization against mode-drift errors, it produces a gate with a theoretical fidelity of 1 for any given gate time τ. We refer to this method as the exact AMFM method. The laser-control pulses $g(t)$ are represented as Fourier-sine series $g(t) = \sum_{n=1}^{N_A} A_n \sin(2\pi n t/\tau)$, where $N_A \sim 1000$ achieves convergence for typical two-qubit gates with $\tau \sim 100$ μs. Thus, in contrast to previous methods that employ either a single [5,7] or a few [32] laser-frequency tones, our method uses a quasicontinuum of frequencies resulting in a chirped pulse of the form $g(t) = \Omega(t)\sin[\psi(t)]$, where $\psi(t) = \int_0^t \mu(t')dt'$ and $\mu(t)$ is the detuning function. The resulting signal can be implemented straightforwardly with an arbitrary waveform generator. Phase-space closure requires $\alpha_p^i = -\eta_p^i \int_0^\tau g(t)\exp(i\omega_p t) = 0$, for $i, p = 1, \ldots, N$, where p is the mode index, i the ion index, η_p^i the Lamb-Dicke parameter, ω_p the mode frequency, and N the number of ions. Therefore, including stabilization against mode-frequency drift to an arbitrary order K, we require $\partial^K \alpha_p^i/\partial\omega_p^K = 0$. This represents $Q = N(K+1)$ homogeneous, linear equations that, in matrix notation, may be written as $M\vec{A}^\gamma = 0$, where $\gamma = 1, \ldots, N_A - Q$ and the set of nontrivial amplitude solutions $\vec{A}^\gamma$ spans the null space of the constraint matrix M. In general, the dimension N_A of the frequency space is much larger than Q, which leaves a large null-space to optimize the gate power. Introducing the root-mean-square (rms) Rabi frequency $\bar{P}$, where $\bar{P}^2 = \langle\Omega^2\rangle = (1/\tau)\int_0^\tau \Omega^2(t)dt = \sum_{n=1}^{N_A} A_n^2$, the gate angle $\chi_{ij} = \vec{A}^T V^{ij}\vec{A}$ is achieved with the minimum $\bar{P}$ if $\vec{A}$ is chosen as the eigenvector of V^{ij} associated with the eigenvalue of largest absolute value. V^{ij} is the null-space projected kernel matrix $\mathcal{K}_{nm}^{ij} = \sum_p \eta_p^i \eta_p^j \int_0^\tau dt_2 \int_0^{t_2} dt_1 \sin(2\pi n t_2/\tau)\sin(2\pi m t_1/\tau) \quad \sin[\omega_p(t_2 - t_1)]$, which can be evaluated analytically since it contains only elementary functions. Since the number of ions N does not occur explicitly other than in the vector space size, the method is naturally scalable to any number of ions. Since the method involves only linear algebra, it is computationally efficient and straightforward to implement. Additional linear conditions, for instance stabilization against gate-timing errors [32], may be added at will. Thus the method also scales in the number and types of stabilization conditions. However, if more conditions are added, the size of the null-space contracts, and with it the number of accessible degrees of freedom, which leads to an increase in the power required. Conversely, for a given set of constraints and $\bar{P}$, there is a minimum gate duration, $\tau_{\min}$, which roughly follows $\tau_{\min} \sim 1/\bar{P}$ for gate times $\tau > 100$ μs. Thus, there is a trade-off between power requirement and gate duration.

Figure 1(a) shows the power requirement of the optimal, exact AMFM method for various qubit pairs (i, j) and degrees of stabilization K as a function of gate duration τ for a 15-ion chain, with an inter-ion spacing of 5 μm and the 11 central ions used as qubits. We see that the power requirement dramatically increases as we decrease τ, exhibiting a steplike transition, whose location is nearly independent of the specific ion pair. The reason is the following. To operate a two-qubit gate at low power,

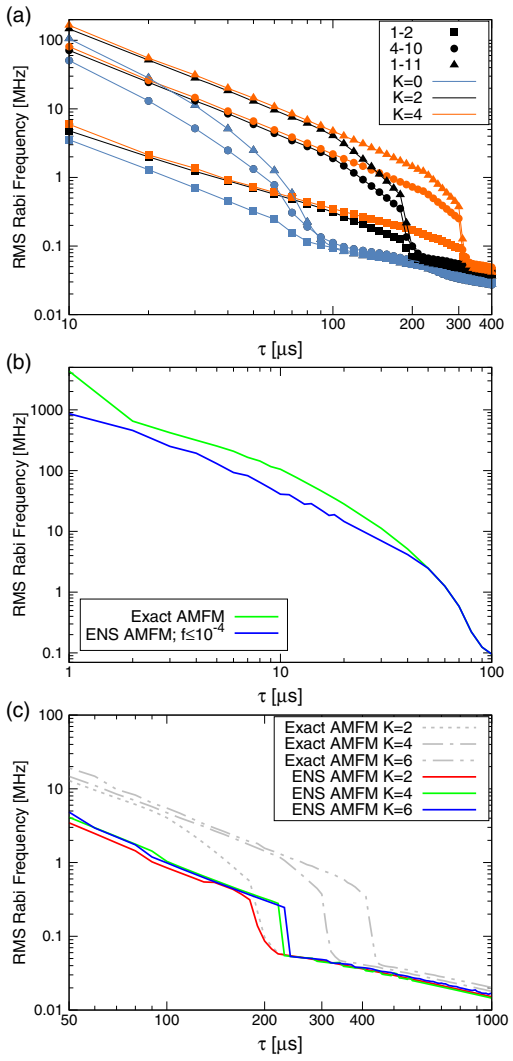

FIG. 1. Properties of gate pulses generated for a 15-ion, 11-qubit chain as a function of gate duration τ. (a) rms Rabi frequency requirement of the exact AMFM gate for three different qubit pairs, (1,2) (squares), (4,10) (circles), and (1,11) (triangles), and three different degrees of stability $K = 0$ (blue), $K = 2$ (black), and $K = 4$ (orange). (b) Comparison between rms Rabi frequency requirement of exact AMFM (green) and ENS AMFM (blue) for $f \leq 10^{-4}$. (c) rms Rabi frequency requirement for different degrees of stabilization K for the ENS protocol (colored, solid lines) with $f \leq 10^{-4}$. Red, green, and blue lines are for $K = 2$, $K = 4$, and $K = 6$, respectively. For comparison, the results for the exact AMFM for $K = 2$ (dotted line) and $K = 4$ (dot-dashed line) are copied from (a) without change, and $K = 6$ (dot-dot-dashed line) is added to illustrate the trend.

it is necessary that the basis frequencies $2\pi nt/\tau$, have good overlap with the motional-mode frequencies, $\omega_p \lesssim 2\pi \times 3$ MHz. As τ decreases, more basis frequencies are pushed out of the frequency range of the motional modes, effectively reducing the dimension of the null space from which the power-optimal solutions are drawn. The step in power results when we run out of null-space vectors with good motional-mode frequency overlap. Since increasing K reduces the null-space dimension even further, the power step happens at larger gate times τ for larger K. Similar to Ref. [33], our scheme cancels carrier excitations to first order due to the sinusoidal nature of our basis functions. While Fig. 1 shows gates < 100 μs, which remain approximately in the Lamb-Dicke regime, further investigation is needed to ensure the standard MS formalism with its perturbative expansions of the Hamiltonian is still valid in this short-pulse regime.

Relaxing the stringent requirement of perfect decoupling between the qubit- and motional-mode states, the AMFM protocol is perfectly suited for implementing the fidelity-power trade-off strategy. This is accomplished by constructing an approximate null space of M that now also includes L_{inc} eigenvectors with nonzero eigenvalues, as long as their moduli are small enough to guarantee $f < f_0$, where f is the infidelity and f_0 is the desired infidelity of the gate. We call this approach the extended null-space (ENS) protocol. The Supplemental Material [39], Sec. S3 contains expanded mathematical detail. Throughout this Letter we use $f_0 = 10^{-4}$, which is deemed acceptable in contemporary experiments, given that it roughly corresponds to the spontaneous scattering limit [40,41].

In Fig. 1(b) we compare the power requirement of ENS AMFM with that of the exact AMFM. We see that ENS AMFM provides a power advantage for $\tau \lesssim 50$ μs. In Fig. 1(c) we compare the pulse-power requirements of stabilized pulses produced according to the exact AMFM method and the ENS method. Over a large span of gate times, the ENS method offers significant power savings for stabilized pulses. In particular, we find that for stability degree $K = 6$ and gate duration $\tau = 250$ μs, the power saving can be as large as a factor of 15.

We note that faster gates come with exponentially decreasing infidelity and increased natural stability against mode-frequency drift, even in the absence of active stabilization. We illustrate this in Fig. 2(a), which shows that increasing the gate speed from 40 to 10 μs reduces the infidelity by about 8 orders of magnitude, reaching below $f = 10^{-11}$ over a drift-frequency range larger than ± 10 kHz at $\tau = 10$ μs. While pulses this short may not be practical, the stability they provide can be propagated to longer gates at the cost of power optimality by reducing the power and repeating the pulse sequence multiple times.

According to Fig. 1(a), qubit pairs that are farther apart from each other require more power. Therefore, given a fixed power budget, instead of trading the power savings afforded by our pulse design for gate duration, we can alternatively trade the savings for better qubit connectivity. This power-connectivity trade-off can play a critical role in harnessing the power of quantum computation since matching hardware and application connectivity is crucial for performance in a future quantum operating system [44]. In Fig. 2(b) we show the power requirement for $K = 4$ and $\tau = 50$ μs pulses as a function of qubit distance for the exact AMFM and the ENS AMFM. We see that compared to its exact AMFM counterpart, ENS AMFM requires factors of about 2 to 4 smaller power.

Experiment.—We implement the exact AMFM and ENS pulses on our programmable, fully connected trapped-ion quantum computer, located at the University of Maryland [45]. We trap seven $^{171}Yb^{+}$ ions in a 1D chain and use the middle five as qubits. The ions are laser-cooled close to the motional ground state, and then optically pumped to $|0\rangle$. Coherent operations are driven by a pair of counterpropagating Raman beams, one of which is split into individual addressing beams, each focused on one ion. These beams are controlled independently by rf pulses generated by arbitrary waveform generators (AWGs), which enable the

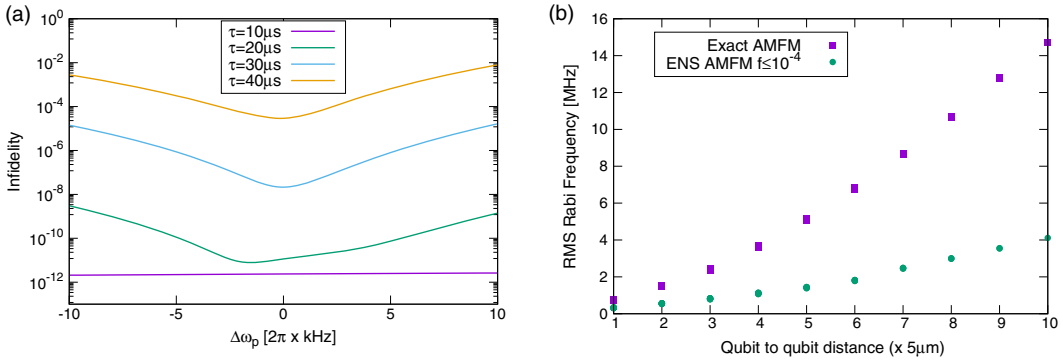

FIG. 2. Trade space for a 15-ion, 11-qubit chain. (a) Infidelity f as a function of uniform mode-frequency drift $\omega_p \to \omega_p + \Delta\omega_p$ on qubits (5,7) ($L_{\mathrm{inc}} = 2$) for four different gate times τ, $K = 0$. (b) rms Rabi frequency requirement as a function of distance between the qubits for a $\tau = 50$ μs gate, $K = 4$. Purple squares: exact AMFM; green circles: ENS AMFM.

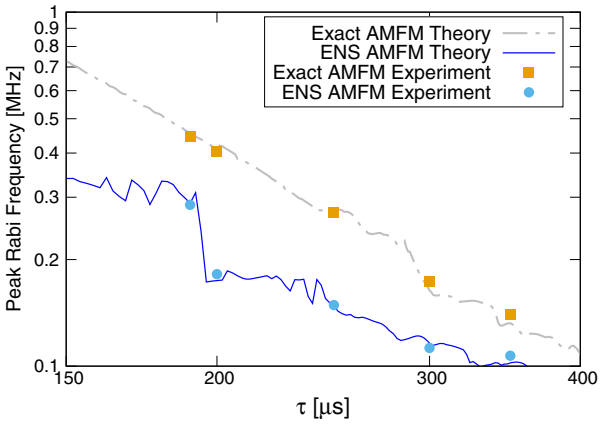

FIG. 3. Comparison of peak power requirements of ENS gates (blue solid line) with exact AMFM gates (gray dashed line) on qubits (4,5) as a function of gate time τ ($K = 4$) for $f \leq 10^{-4}$ on a seven-ion, five-qubit chain. Experimental results for different gate times, implementing pulses constructed according to the exact AMFM and ENS protocols, are shown as orange squares and blue circles, respectively. The experimental error bars are smaller than the plot symbols.

implementation of pulse shapes from a broad range of frequencies, amplitudes, and phases.

Figure 3 shows the theoretically predicted and experimentally measured power requirements as a function of gate duration for exact AMFM and ENS-based pulses. We chose $f_0 = 10^{-4}$ since the experimental gates are limited to $\sim 10^{-2}$ by other imperfections with the leading sources of error being intensity and phase noise on the Raman beams, caused by beam-steering fluctuations and imperfect overlap of the beam and ion positions. We chose to stabilize these pulses to degree $K = 4$. Because of the limited amplitude resolution of the AWG (14-bit DAC), the relative amplitudes of basis frequencies smaller than 10^{-4} are neglected in the experimental implementation. We confirmed numerically that this does not significantly impact the theoretical fidelity and stability of the resulting gates. We verify a successful implementation of a pulse by observing a continuous coherent transfer of population between the $|00\rangle$ and $|11\rangle$ states when the applied laser power is varied. We then calculate the minimal Rabi frequency $\Omega_0 = s\Omega_{\max}$ needed to perform a maximally entangling gate, where $s \leq 1$ is a scale factor on the AWG amplitude, used to set the Rabi frequency with the help of a controller calibration curve, and $\Omega_{\max}$ is the maximum Rabi rate measured at the ions. We further verify the creation of the maximally entangled state by measuring the parity contrast for some of the pulses [7].

All the experimentally determined Rabi frequencies for the two-qubit gates, using either the ENS- or the exact AMFM protocols, fall within $\pm 10\%$ of the respective theoretically predicted values. The small discrepancies between experimental values and theory predictions are due to uncertainties in the Lamb-Dicke parameters and mode frequencies (see Supplemental Material [39], Sec. S4). We note that shorter gates at higher Rabi frequency may suffer from more noise, and thus higher infidelity due to, e.g., acoustic vibrations, which do not get averaged out over the gate application.

We demonstrate the benefit of stabilizing the gates with respect to fluctuations in the motional-mode frequencies by applying pulses with two different stabilization orders, i.e., $K = 1$ and $K = 5$, to qubits (4,5) on our seven-ion, five-qubit quantum computer. The two ENS AMFM pulses are constructed with $f_0 = 10^{-4}$ at zero gate-frequency offset. To systematically control the detuning error, we offset the gate frequency from the original intended gate frequency, which is equivalent to uniformly offsetting the motional-mode frequencies in the opposite direction. We apply the pulses to the initial state $|00\rangle$ and measure the even-parity populations when $P_{00} \approx P_{11}$, akin to performing a maximally entangling gate. Figure 4 shows the even-parity population $P_{\text{even}} = P_{00} + P_{11}$, which is the quantity stabilized by the gate. Since this does not measure coherent errors, we checked the parity contrast for some of the pulses as for the previous measurement. The experimentally measured values with their associated error bars are marked in red. The error bars are 1σ confidence intervals, sampled from a binomial distribution, and each point represents 4000 experimental shots. The blue line shows the analytical fidelity $\bar{F} = 1 - \frac{4}{5}\sum_p (|\alpha_{i,p}|^2 + |\alpha_{j,p}|^2)$, which is valid in the low-infidelity limit [41]. As expected, the width of the detuning-robust region is larger for the pulse with the higher stabilization order.

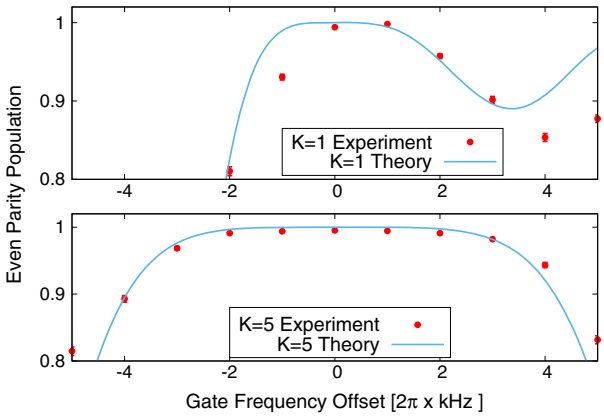

FIG. 4. Experimental demonstration of the K-order stabilized two-qubit gates for qubit pair (4,5) on our seven-ion, five-qubit quantum computer. The ENS AMFM pulse sequence satisfying $f \leq 10^{-4}$ at no frequency offset with $K = 1$ (top) and $K = 5$ (bottom), corresponds to a maximally entangling gate. The experimentally measured even-parity population is plotted as a function of the gate frequency. The blue lines show the gate fidelity according to the analytical expression for $\bar{F}$, valid in the low-error limit. The width of the detuning-robust region is larger for the pulse with the higher stabilization order ($K = 5$ vs $K = 1$).

Outlook.—The impossible trinity formed by power, gate duration, and fidelity, discussed and illustrated in this Letter, has an analog in the chip design community, where there are well-known fundamental trade-offs between power, performance, and area, commonly referred to as PPA (see, e.g., Ref. [46]). Given that the physical-level infidelity affects, for instance, the cost of implementing quantum error correction to achieve a target logical-level infidelity, our investigations could be considered a quantum version of PPA trade-offs. Given the enormous utility and impact of a careful PPA study for system-on-a-chip design, our results may contribute to future quantum processor optimization. We are convinced that this holistic optimization of all facets of the design based on the PPA trade-off is another stepping stone toward successful practical quantum computing.

We thank Cinthia Huerta Alderete and Yingyue Zhu for help with the experiment. N. M. L. acknowledges financial support from the NSF Grant No. PHY-1430094 to the Physics Frontier Center at the Joint Quantum Institute, and the University of Maryland - Army Research Laboratory Quantum Partnership, Grant No. W911NF1920181. A. M. G. is supported by a JQI Postdoctoral Fellowship.

[1] F. Arute *et al.*, Quantum supremacy using a programmable superconducting processor, Nature (London) **574**, 505 (2019).
[2] https://www.ibm.com/quantum-computing/ (Accessed September 13, 2020).
[3] https://www.rigetti.com (Accessed September 13, 2020).
[4] https://www.honeywell.com/en-us/company/quantum (Accessed September 13, 2020).
[5] K. Wright *et al.*, Benchmarking an 11-qubit quantum computer, Nat. Commun. **10**, 5464 (2019).
[6] P. Schindler, D. Nigg, T. Monz, J. T. Barreiro, E. Martinez, S. X. Wang, S. Quint, M. F. Brandl, V. Nebendahl, C. F. Roos, M. Chwalla, M. Hennrich, and R. Blatt, A quantum information processor with trapped ions, New J. Phys. **15**, 123012 (2013).
[7] T. Choi, S. Debnath, T. A. Manning, C. Figgatt, Z.-X. Gong, L.-M. Duan, and C. Monroe, Optimal Quantum Control of Multimode Couplings between Trapped Ion Qubits for Scalable Entanglement, Phys. Rev. Lett. **112**, 190502 (2014).
[8] V. Kaushal *et al.*, Shuttling-based trapped-ion quantum information processing, AVS Quantum Sci. **2**, 014101 (2020).
[9] S. S. Elder, C. S. Wang, P. Reinhold, C. T. Hann, K. S. Chou, B. J. Lester, S. Rosenblum, L. Frunzio, L. Jiang, and R. J. Schoelkopf, High-Fidelity Measurement of Qubits Encoded in Multilevel Superconducting Circuits, Phys. Rev. X **10**, 011001 (2020).
[10] J. I. Colless, V. V. Ramasesh, D. Dahlen, M. S. Blok, M. E. Kimchi-Schwartz, J. R. McClean, J. Carter, W. A. de Jong, and I. Siddiqi, Computation of Molecular Spectra on a Quantum Processor with an Error-Resilient Algorithm, Phys. Rev. X **8**, 011021 (2018).
[11] https://github.com/Qiskit/ibmq-device-information (Accessed September 12, 2020).
[12] https://pyquil-docs.rigetti.com/en/stable/compiler.html#compiler (Accessed September 12, 2020).
[13] D. Maslov, Basic circuit compilation techniques for an ion-trap quantum machine, New J. Phys. **19**, 023035 (2017).
[14] C. D. Bruzewicz, J. Chiaverini, R. McConnell, and J. M. Sage, Trapped-ion quantum computing: Progress and challenges, Appl. Phys. Rev. **6**, 021314 (2019).
[15] https://aws.amazon.com/braket/hardware-providers/rigetti/ (Accessed September 12, 2020).
[16] Y. Nam *et al.*, Ground-state energy estimation of the water molecule on a trapped-ion quantum computer, npj Quantum Inf. **6**, 33 (2020).
[17] D. Leibfried, B. DeMarco, V. Meyer, D. Lucas, M. Barrett, J. Britton, W. M. Itano, B. Jelenković, C. Langer, T. Rosenband, and D. J. Wineland, Experimental demonstration of a robust, high-fidelity geometric two ion-qubit phase gate, Nature (London) **422**, 412 (2003).
[18] K. Mølmer and A. Sørensen, Multiparticle Entanglement of Hot Trapped Ions, Phys. Rev. Lett. **82**, 1835 (1999).
[19] A. Sørensen and K. Mølmer, Entanglement and quantum computation with ions in thermal motion, Phys. Rev. A **62**, 022311 (2000).
[20] G. J. Milburn, S. Schneider, and D. F. V. James, Ion trap quantum computing with warm ions, Fortsch. Phys. **48**, 801 (2000).
[21] J. P. Gaebler, T. R. Tan, Y. Lin, Y. Wan, R. Bowler, A. C. Keith, S. Glancy, K. Coakley, E. Knill, D. Leibfried, and D. J. Wineland, High-Fidelity Universal Gate Set for $^{9}Be^{+}$ Ion Qubits, Phys. Rev. Lett. **117**, 060505 (2016).
[22] C. J. Ballance, T. P. Harty, N. M. Linke, M. A. Sepiol, and D. M. Lucas, High-Fidelity Quantum Logic Gates Using Trapped-Ion Hyperfine Qubits, Phys. Rev. Lett. **117**, 060504 (2016).
[23] S.-L. Zhu, C. Monroe, and L.-M. Duan, Trapped Ion Quantum Computation with Transverse Phonon Modes, Phys. Rev. Lett. **97**, 050505 (2006).
[24] S.-L. Zhu, C. Monroe, and L.-M. Duan, Arbitrary-speed quantum gates within large ion crystals through minimum control of laser beams, Europhys. Lett. **73**, 485 (2006).
[25] G. Zarantonello, H. Hahn, J. Morgner, M. Schulte, A. Bautista-Salvador, R. F. Werner, K. Hammerer, and C. Ospelkaus, Robust and Resource-Efficient Microwave Near-Field Entangling $^{9}Be^{+}$ Gate, Phys. Rev. Lett. **123**, 260503 (2019).
[26] C. F. Roos, Ion trap quantum gates with amplitude-modulated laser beams, New J. Phys. **10**, 013002 (2008).
[27] T. J. Green and M. J. Biercuk, Phase-Modulated Decoupling and Error Suppression in Qubit-Oscillator Systems, Phys. Rev. Lett. **114**, 120502 (2015).
[28] D. Hayes, S. M. Clark, S. Debnath, D. Hucul, I. V. Inlek, K. W. Lee, Q. Quraishi, and C. Monroe, Coherent Error Suppression in Multiqubit Entangling Gates, Phys. Rev. Lett. **109**, 020503 (2012).
[29] A. R. Milne, C. L. Edmunds, C. Hempel, F. Roy, S. Mavadia, and M. J. Biercuk, Phase-Modulated Entangling

Gates Robust to Static and Time-Varying Errors, Phys. Rev. Applied **13**, 024022 (2020).
[30] P. H. Leung, K. A. Landsman, C. Figgatt, N. M. Linke, C. Monroe, and K. R. Brown, Robust 2-Qubit Gates in a Linear Ion Crystal Using a Frequency-Modulated Driving Force, Phys. Rev. Lett. **120**, 020501 (2018).
[31] R. Blümel, N. Grzesiak, and Y. Nam, Power-optimal, stabilized entangling gate between trapped-ion qubits, arXiv:1905.09292.
[32] Y. Shapira, R. Shaniv, T. Manovitz, N. Akerman, and R. Ozeri, Robust Entanglement Gates for Trapped-Ion Qubits, Phys. Rev. Lett. **121**, 180502 (2018).
[33] V. M. Schäfer, C. J. Ballance, K. Thirumalai, L. J. Stephenson, T. G. Ballance, A. M. Steane, and D. M. Lucas, Fast quantum logic gates with trapped-ion qubits, Nature (London) **555**, 75 (2018).
[34] N. Grzesiak *et al.*, Efficient arbitrary simultaneously entangling gates on a trapped-ion quantum computer, Nat. Commun. **11**, 2963 (2020).
[35] C. Figgatt, A. Ostrander, N. M. Linke, K. A. Landsman, D. Zhu, D. Maslov, and C. Monroe, Parallel entangling operations on a universal ion-trap quantum computer, Nature (London) **572**, 368 (2019).
[36] Y. Lu, S. Zhang, K. Zhang, W. Chen, Y. Shen, J. Zhang, J.-N. Zhang, and K. Kim, Global entangling gates on arbitrary ion qubits, Nature (London) **572**, 363 (2019).
[37] D. Leibfried, E. Knill, C. Ospelkaus, and D. J. Wineland, Transport quantum logic gates for trapped ions, Phys. Rev. A **76**, 032324 (2007).
[38] C. Ospelkaus, C. E. Langer, J. M. Amini, K. R. Brown, D. Leibfried, and D. J. Wineland, Trapped-ion Quantum Logic Gates Based on Oscillating Magnetic Fields, Phys. Rev. Lett. **101**, 090502 (2008).
[39] See Supplemental Material at http://link.aps.org/supplemental/10.1103/PhysRevLett.126.220503 for more details on the experimental setup, pulse shapes, and the protocol used to accurately determine the Lamb-Dicke parameters, which includes Refs. [31,40–43].
[40] N. C. Brown and K. R. Brown, Comparing Zeeman qubits to hyperfine qubits in the context of the surface code: $^{174}Yb^{+}$ and $^{171}Yb^{+}$, Phys. Rev. A **97**, 052301 (2018).
[41] Y. Wu, S.-T. Wang, and L.-M. Duan, Noise analysis for high-fidelity quantum entangling gates in an anharmonic linear Paul trap, Phys. Rev. A **97**, 062325 (2018).
[42] D. J. Wineland, C. Monroe, W. M. Itano, D. Leibfried, B. E. King, and D. M. Meekhof, Experimental issues in coherent quantum-state manipulation of trapped atomic ions, J. Res. Natl. Inst. Stand. Technol. **103**, 259 (1998).
[43] S.Olmschenk, K. C. Younge, D. L. Moehring, D. N. Matsukevich, P.Maunz, and C. Monroe, Manipulation and detection of a trapped Yb^{+} hyperfine qubit, Phys. Rev. A **76**, 052314 (2007).
[44] N. M. Linke, D. Maslov, M. Roetteler, S. Debnath, C. Figgatt, K. A. Landsman, K. Wright, and C. Monroe, Experimental comparison of two quantum computing architectures, Proc. Natl. Acad. Sci. U.S.A. **114**, 3305 (2017).
[45] K. A. Landsman, C. Figgatt, T. Schuster, N. M. Linke, B. Yoshida, N. Y. Yao, and C. Monroe, Verified quantum information scrambling, Nature (London) **567**, 61 (2019).
[46] A. Teman, D. Rossi, P. A. Meinerzhagen, L. Benini, and A. P. Burg, Power, area, and performance optimization of standard cell memory arrays through controlled placement, ACM Trans. Des. Automat. Electron. Syst. **21**, 59 (2016).